Kobe University Repository : Kernel

PDF issue: 2024-09-27

Combined analysis of energy band diagram and equivalent circuit on nanocrystal solid

Kano, Shinya

Sasaki, Masato

Fujii, Minoru

(Citation)
Journal of Applied Physics,119(21):215304-215304

(Issue Date)
2016-06-07

(Resource Type)
journal article

(Version)
Version of Record

(Rights)
©2016 AIP Publishing. This article may be downloaded for personal use only. Any other use requires prior permission of the author and AIP Publishing. The following article appeared in Journal of Applied Physics 119(21), 215304 and may be found at http://dx.doi.org/10.1063/1.4953216

(URL)
https://hdl.handle.net/20.500.14094/90003531

Combined analysis of energy band diagram and equivalent circuit on nanocrystal solid
Shinya Kano, Masato Sasaki, and Minoru Fujii

Citation: Journal of Applied Physics **119**, 215304 (2016); doi: 10.1063/1.4953216
View online: http://dx.doi.org/10.1063/1.4953216
View Table of Contents: http://aip.scitation.org/toc/jap/119/21
Published by the American Institute of Physics

Articles you may be interested in
Integration of colloidal silicon nanocrystals on metal electrodes in single-electron transistor
Applied Physics Letters **109**, 213104 (2016); 10.1063/1.4968583

AIP | Journal of Applied Physics
Save your money for your research.
It's now FREE to publish with us -
no page, color or publication charges apply.
Publish your research in the
Journal of Applied Physics
to claim your place in applied
physics history.

Combined analysis of energy band diagram and equivalent circuit on nanocrystal solid

Shinya Kano,[a] Masato Sasaki, and Minoru Fujii[a]
Department of Electrical and Electronic Engineering, Graduate School of Engineering, Kobe University, Rokkodai, Nada, Kobe 657-8501, Japan

(Received 6 April 2016; accepted 21 May 2016; published online 3 June 2016)

We investigate a combined analysis of an energy band diagram and an equivalent circuit on nanocrystal (NC) solids. We prepared a flat silicon-NC solid in order to carry out the analysis. An energy band diagram of a NC solid is determined from DC transport properties. Current-voltage characteristics, photocurrent measurements, and conductive atomic force microscopy images indicate that a tunneling transport through a NC solid is dominant. Impedance spectroscopy gives an equivalent circuit: a series of parallel resistor-capacitors corresponding to NC/metal and NC/NC interfaces. The equivalent circuit also provides an evidence that the NC/NC interface mainly dominates the carrier transport through NC solids. Tunneling barriers inside a NC solid can be taken into account in a combined capacitance. Evaluated circuit parameters coincide with simple geometrical models of capacitances. As a result, impedance spectroscopy is also a useful technique to analyze semiconductor NC solids as well as usual DC transport. The analyses provide indispensable information to implement NC solids into actual electronic devices. *Published by AIP Publishing.*
[http://dx.doi.org/10.1063/1.4953216]

I. INTRODUCTION

Semiconductor nanocrystal (NC) has been intensively studied in the field of nanomaterials for decades due to the unique electronic and opto-electronic properties.[1–4] A semiconductor NC solid has a potential application in solution–processed electronic devices, such as a photodetector, field-effect transistor, and solar cell.[5] Carrier transport of the NC solid in electronic devices can be strongly dependent on the interface of semiconductor NCs. For example, tunneling barriers of a NC surface caused by a slight oxidation impede the transport of charge carriers.[6,7] Various mechanisms of the carrier transport through NCs have been proposed: for example, variable range hopping,[8,9] Fowler-Nordheim tunneling,[10] and Poole-Frenkel emission.[11,12] Traditionally, these analyses are based on carrier dynamics in energy band diagrams.

Impedance spectroscopy has been recently used to find an equivalent electrical circuit of nanomaterial devices.[13–16] Sugiyama *et al.* suggested an application of impedance spectroscopy to Cu(In, Ga)Se_2-based solar cells because an equivalent circuit can be affected by defects around material interfaces.[16] Huh *et al.* evaluated a Schottky contact between a SnO_2 nanowire and a metal electrode by using equivalent electrical circuit.[13] However, limited research articles have shown an impedance analysis on NC solids.[12,17] In addition, correspondence of an equivalent electrical circuit to an energy band diagram on a NC solid has not been shown. For example, it is not clear how to treat tunneling barriers inside a NC solid as a capacitance quantitatively. It is meaningful to understand the correspondence by using impedance spectroscopy in order to design electronic devices based on NC solids.

In this article, we analyze electrical properties of NC solids by using both an energy band diagram and an equivalent circuit. We form a flat solid by using a completely dispersed NC colloid and investigate the current transport by using these two viewpoints. An energy band diagram of the NC solid is discussed by analyzing DC-voltage characteristics and a photocurrent generation of NC solids. Impedance spectroscopy is carried out to express the NC solid as an equivalent circuit. We discuss the validity of an estimated equivalent circuit.

II. EXPERIMENTAL

Among various elements of semiconductor NCs, silicon (Si) NCs are recently investigated intensively because of the high compatibility to the complementary metal-oxide semiconductor (CMOS) technology.[9,18–22] We have recently developed a colloidal Si NC having heavily boron (B) and phosphorus (P) codoped shells.[23–28] The codoped Si NC is dispersible in polar solvents without organic ligands because of a negative electrostatic potential induced on the surface.[23] NC solids made from the colloids have very high flatness in a wide range, allowing us to study the transport properties in detail.[29]

Colloidal B and P codoped Si NCs were prepared using a co-sputtering method described in our previous papers.[23–25] Si-rich borophosphosilicate films were deposited on a stainless steel plate by co-sputtering Si, SiO_2, B_2O_3, and P_2O_5. After removal from the stainless steel plate, the films were annealed in a N_2 atmosphere at 1200 °C for 30 min. Codoped Si NCs were grown in the films by annealing. Then, the films were mixed with hydrofluoric acid (46 wt. %) to etch SiO_2

[a]Authors to whom correspondence should be addressed. Electronic addresses: kano@eedept.kobe-u.ac.jp and fujii@eedept.kobe-u.ac.jp

matrices and extract the Si NCs. The Si NCs were centrifuged and transferred into methanol. Concentration of colloidal Si NCs was 0.4–0.5 mg/ml. The surface of Si NCs was slowly oxidized during storage in methanol. The thickness of the surface oxides is estimated to be 1 nm at most.[26] Figure 1(a) shows a photograph of finished colloidal Si-NC solution. Clear solution without any agglomerates can be obtained because the Si NC in the solution is well dispersed. This dispersion is important to fabricate a flat NC solid on a substrate. Figure 1(b) shows a transmission electron microscopy (TEM) image of codoped Si NCs annealed at 1200 °C. An average diameter of NCs is estimated to be $D = 7$ nm in our previous report.[24]

A fabrication method of a Si-NC solid is as follows. Colloidal Si-NC solution was spin-coated on an indium-tin-oxide (ITO, 90 nm)/glass substrate, which was cleaned up by ultrasonication with alcohol and UV/O_3 treatments. The thickness of the spin-coated solids was measured by a stylus profiler (DektakXT, BRUKER Corporation) and was 50 nm. Aluminum (Al) electrodes (area $A = 1.1 \times 10^{-6}$ m^2, thickness $t = 100$ nm) were thermally deposited on the solid. It is noted that the Si-NC solids were not intentionally etched and sintered prior to the Al deposition, and thus the Si NCs do not coalesce each other. Topography and local conductivity of the solids were obtained by a conductive atomic force microscopy (AFM) using a rhodium (Rh)-coated cantilever at ambient condition (HITACHI High-Tech Science, E-sweep). Topographic and conductive images of the solids were visualized by using Gwyddion.[30]

Figure 1(c) shows a schematic illustration of a device structure under investigation. Current-voltage characteristics were taken by a source measure unit (Keithley, 236) at ambient condition. The accuracy of DC measurement was 0.3%. Photocurrent was obtained by illuminating the sample with a 405-nm semiconductor laser module. The illuminated area was approximately 2–3 mm in diameter. Impedance spectroscopy was carried out by using LCR meter (NF Corporation, ZM2376). Frequency of AC voltage was changed from 1 Hz to 1 MHz. An AC voltage was constant at 10 mV through all measurements. The accuracy of impedance was estimated to be several tens of % at most, which is good enough to evaluate the equivalent circuit.

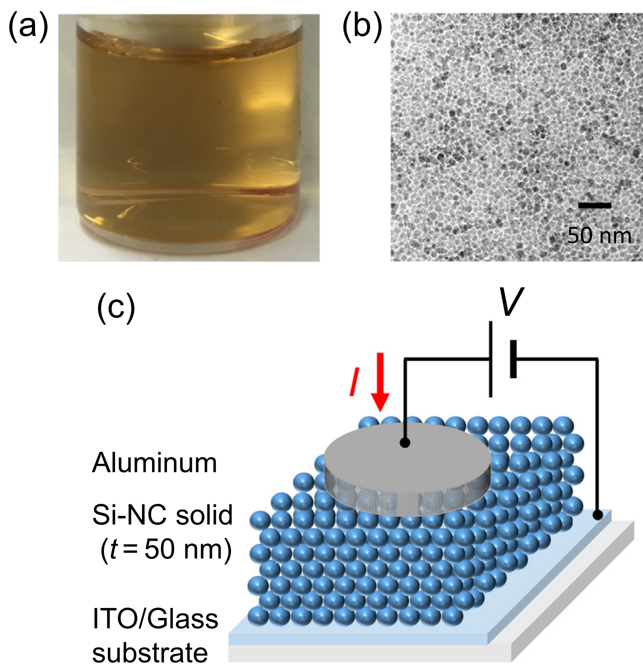

FIG. 1. (a) Photograph of colloidal Si NCs in methanol. (b) TEM image of Si NCs. (c) Schematic illustration of a device under investigation. A bias voltage is applied from ITO to Al electrode.

III. RESULTS AND DISCUSSION

Figure 2(a) shows a linear plot of a current-voltage characteristic of a device in Fig. 1(c). In a lower voltage region ($-1.0 < V < 0$ V), a current is proportional to a bias voltage. Since a very thin oxide layer surrounding NCs works as a tunneling barrier, this current can be attributed to a tunneling phenomenon. It is known that a tunneling current through a thin insulator is linearly proportional to a bias voltage in a small voltage region.[31] In a higher voltage region ($V < -1.0$ V), a current increases rapidly.

Figure 2(b) shows a Fowler-Nordheim plot ($\ln(J/V^2)$ $-1/|V|$) of the current-voltage characteristics. The dependence of a current density J versus V in a Fowler-Nordheim tunneling model is described as[32]

$$|J| \propto |V|^2 \exp\left(-\frac{1}{|V|}\right). \tag{1}$$

Because a straight line can be well fitted in $|V| > 1.0$ V of Fig. 2(b), we clearly see a Fowler-Nordheim tunneling process contributes to the current transport in this region. The electric field in the tunneling barrier between Si NCs is 1 MV/cm at $|V| = 1.5$ V if an applied voltage is divided in every Si-NC shells (shell thickness ~1 nm (Ref. 27)) equally. This high electric field can be attributed to the Fowler-Nordheim tunneling regime.

Figure 3(a) shows a current response of a Si-NC solid under light irradiation ($\lambda = 405$ nm, 3.3 mW) as a function of time. Conductance of NC solids increases under the illumination because an electron and hole pair is generated inside the Si NC. The increment of the conductivity by a light irradiation is much weaker at longer wavelength (786 nm) due to smaller absorption of Si-NCs (Figure S1). A time constant of the device in this measurement is estimated to be about 3 s (Figure S2). The validity of the time constant will be discussed later.

Figure 3(b) shows current-voltage characteristics as a function of light intensity. In general, photocurrent I_{ph} increases with light intensity F following a power law as $I_{ph} \propto F^{\gamma}$.[7] Here, I_{ph} is the difference between a current measured under illumination and a dark current. Figure 3(c) describes a relationship between γ and V. As the applied voltage increases, the value of γ increases from ~0.1 to unity over $|V| > 1.0$ V, which means excited carriers can be extracted from the solids more efficiently. Because the voltage where the Fowler-Nordheim tunneling appears is also $|V| > 1.0$ V,

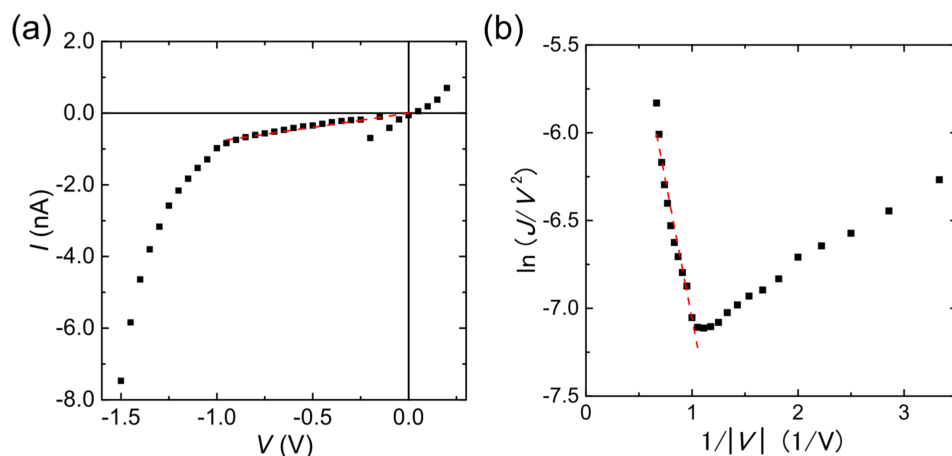

FIG. 2. Current-voltage characteristics of a device in Fig. 1(c) at room temperature. (a) Linear and (b) Fowler-Nordheim plots. Dashed lines are linear fit lines.

the Fowler-Nordheim tunneling possibly enhances the carrier extraction in this voltage region.

Current images of a Si-NC solid by conductive AFM support the tunneling mechanism of carrier transport. Conductive AFM can obtain a local conductance mapping of nanomaterial films.[33–35] Figure 4(a) shows a local topographic image of a Si-NC solid. A surface roughness of the solid is about 10 nm, corresponding to a length of a few number of NCs in series. This image supports the formation of a flat NC solid. Figures 4(b)–4(d) show a conductance mapping of the Si-NC solid by applying $V = 0$, -6, and -10 V, respectively. As increasing V, a conductance mapping similar to Fig. 4(a) can be obtained. We can see a lower topographic area gives higher conductance, which is a similar tendency of a polycrystalline NiO insulator.[35] In addition, a small current less than 10 pA is observed on the top of a Si NC solid in Fig. 4(d) although $V = -10$ V is applied. This image indicates that the intensity of current decays exponentially as increasing the thickness of a solid ($I \propto \exp(-\alpha d)$, where α is a decay constant and d is the thickness). This tendency supports that a tunneling transport is dominant through the Si-NC solid.

In Fig. 5, we summarize a band diagram of a Si-NC solid. Valence band edge (5.0 eV) and conduction band edge (4.0 eV) in 7-nm diameter of Si NCs have been estimated by using photoelectron yield spectroscopy and valence band

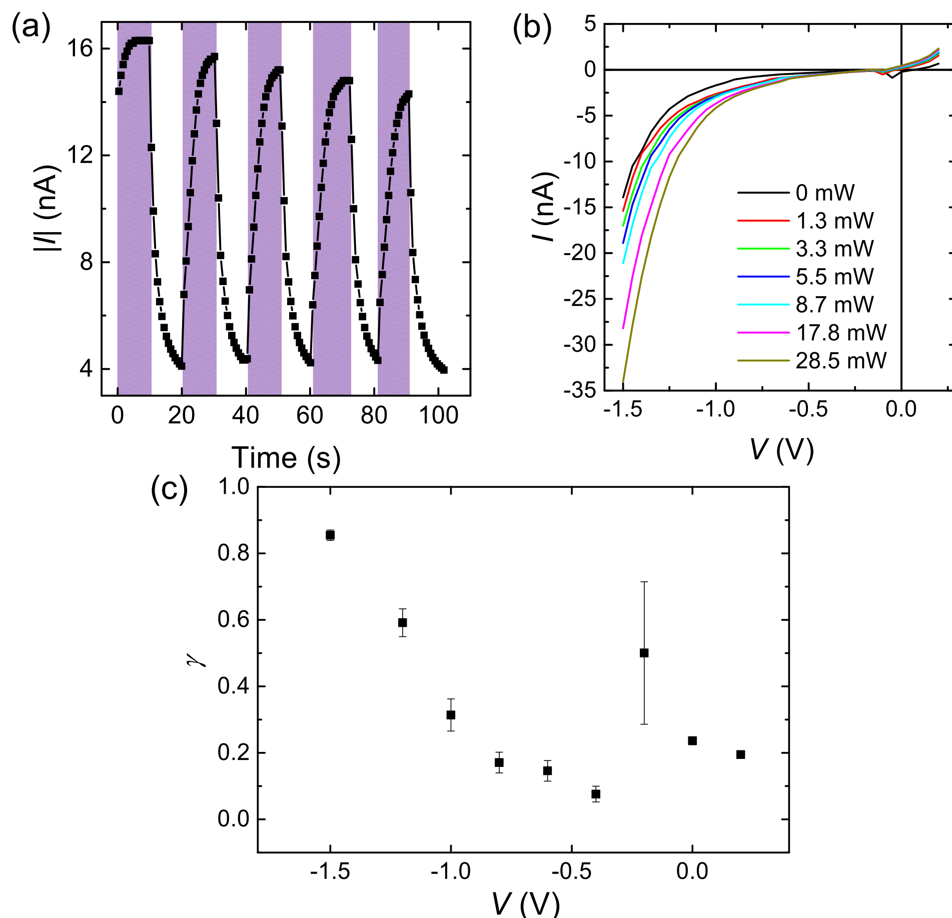

FIG. 3. (a) Current response of Si-NC solids with light irradiation ($\lambda = 405$ nm, 3.3 mW) at $V = -0.1$ V. Colored and non-colored regions correspond to the response with and without the irradiation, respectively. (b) I—V characteristics with light irradiation. (c) Exponent factor ($I_{ph} \propto F^{\gamma}$) calculated in each constant voltage.

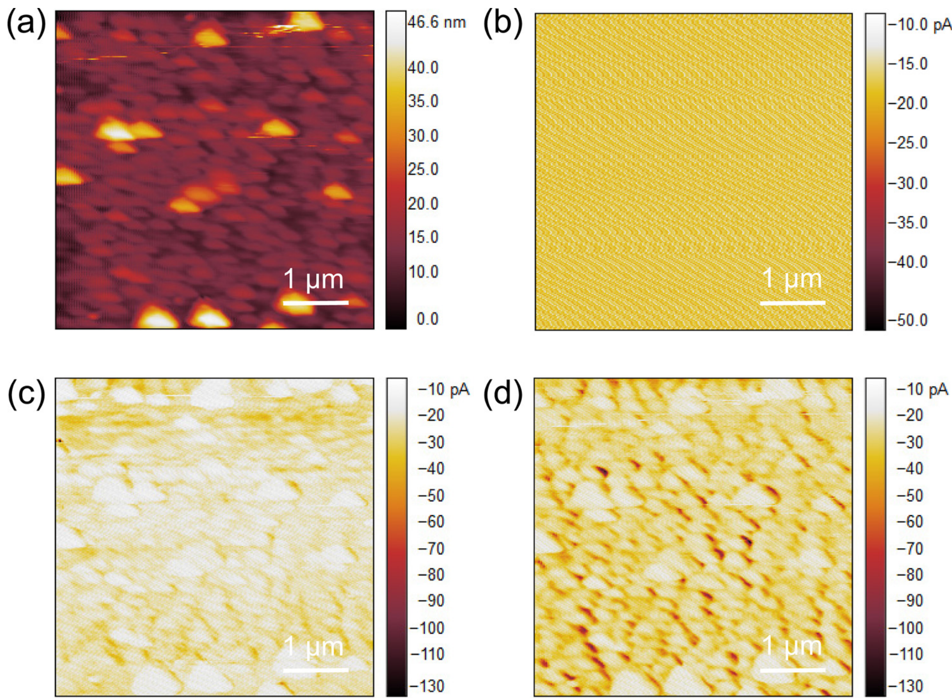

FIG. 4. (a) Topographic image and (b)–(d) current image of colloidal Si-NC solid/ITO substrate observed by conductive AFM. Bias voltage V is applied to ITO as (b) $V=0$ V, (c) $V=-6$ V, and (d) $V=-10$ V.

spectra.[28] The small value of the band gap (∼1.0 eV) is due to heavy doping of B and P in Si NCs.[24] When no voltage is applied ($V=0$ V, Fig. 5(a)), an offset voltage appears corresponding to the difference of work function between Al and ITO. This offset voltage is expected to be 0.6 eV; however, only 0.2 V of the offset voltage is observed in Fig. 2(a). This difference is probably attributed to the trapped charge in interface states between NC solids and metal electrodes.

When $|V|<1.0$ V (low voltage regime, Fig. 5(c)), carriers in metal are injected via simple tunneling process through tunneling barriers of codoped Si-NC shells. As $|V|>1.0$ V (high voltage regime, Fig. 5(d)), the Fowler-Nordheim tunneling starts to appear through a conduction band of the tunneling barrier. A higher voltage enhances a mean free path of carriers, and thus, the carriers irradiated by photon flux move more efficiently.

Here, we show an impedance spectroscopy of a Si-NC solid. We discuss a relationship between the band diagram in Fig. 5(a) and an equivalent circuit of the structure.

Figure 6(a) shows complex-plane impedance plots of a device in Fig. 1(c) in ambient condition. Filled square and filled circle express experimental and theoretically simulated results, respectively. The inclined experimental curve indicates that a NC solid consists of both capacitance and resistance components, as shown in a previous report.[36] Here, we fit a theoretical impedance plot using an electrical circuit

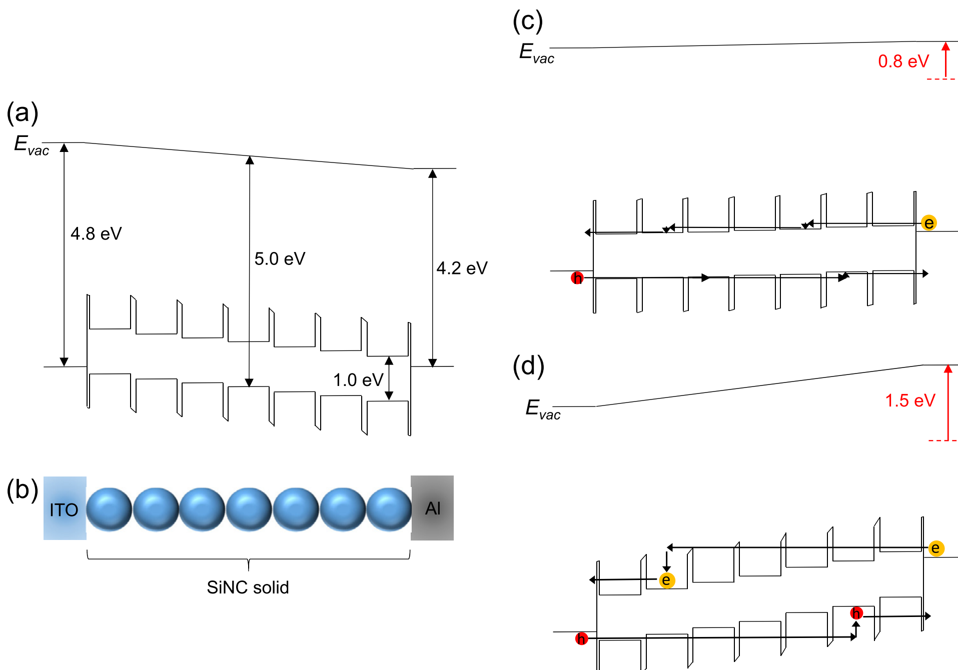

FIG. 5. Band diagram of a Si-NC solid. (a) Under $V=0$ V and (b) corresponding schematic illustration of the structure. (c) Under $V=-0.8$ V (low voltage regime), and (d) $V=-1.5$ V (high voltage regime).

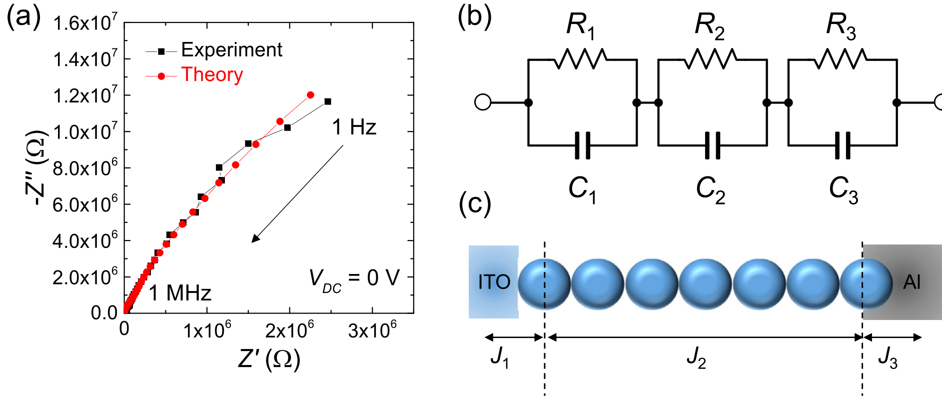

FIG. 6. (a) Impedance plots of a device in Fig. 1(c) at ambient condition. A DC bias $V_{DC} = 0$ V is applied to the device. (b) Equivalent circuit of a device in Fig. 1(c). (c) Definition of each junction J_i ($i = 1$, 2, and 3) in a schematic model.

model in Fig. 6(b): parallel resistor-capacitors 1–3 in series corresponding to ITO/NC, NC/NC, and NC/Al interfaces, respectively (Fig. 6(c)). In this model, we consider a NC solid as a continuum insulator, and then resistor-capacitor networks are combined into a single parallel resistor-capacitor model.

Impedance of the circuit in Fig. 6(b) is described as follows:

$$
\begin{aligned}
Z &= Z' + iZ'' \\
&= \frac{R_1}{1+(\omega C_1 R_1)^2} + \frac{R_2}{1+(\omega C_2 R_2)^2} + \frac{R_3}{1+(\omega C_3 R_3)^2} \\
&\quad - i\left(\frac{\omega C_1 R_1^2}{1+(\omega C_1 R_1)^2} + \frac{\omega C_2 R_2^2}{1+(\omega C_2 R_2)^2} + \frac{\omega C_3 R_3^2}{1+(\omega C_3 R_3)^2}\right),
\end{aligned}
\tag{2}
$$

where ω is an angular frequency, and R_j and C_j are resistance and capacitance of jth junction ($j = 1$, 2, and 3). Evaluated parameters from Fig. 6(a) are shown in Table I.

The value of R_2 is more than a hundred times larger than those of R_1 and R_3. This is due to serially connected 5–7 tunneling barriers between Si NCs as shown in Fig. 6(c). This result indicates that tunneling barriers exist in a Si-NC solid. The values of resistance R_1 and R_3 might be related to difference of Fermi levels between a NC solid and metals.

It is noted that the experimental difference between C_1 and C_3 is possibly attributed to the morphology of electrode/NC junctions. In case of an Al/Si NC junction, the Al electrode covers the surface of NCs because of the thermal evaporation process as shown in Fig. 6(c). In contrast, the ITO electrode under Si NCs ideally contacts on the top of NCs since the NCs are just spin-coated. The capacitance value of C_3 can be slightly larger than that of C_1, and we assign the Al electrode to the larger capacitance junction (J_3) in Fig. 6(c).

Capacitances C_1 and C_3 between the NC solid and the metals are evaluated by using a mutual capacitance between a Si NC in 7-nm diameter and a metal. Mutual capacitance between a single sphere and an infinite conductive plane can be evaluated as

$$C = 4\pi\epsilon r \sinh\alpha \sum_{n=1}^{\infty} \frac{\mathbf{1}}{\sinh n\alpha}, \tag{3}$$

where r is a radius of a sphere, ϵ is a dielectric constant of a medium, α is defined to be acosh(d/r), and d is a distance between the center of a sphere and the surface of a conductive plane, respectively (Figure S3(a)).[37] Combined capacitance of all NCs against a metal is estimated to be 91 nF at maximum, which is 1.1–1.7 times larger than the experimental C_1 and C_3 (the detailed calculation is shown in the supplementary material).[38] In our previous study, an experimental fill factor of drop-coated NC solids was 35%.[27] This difference between experimental and theoretical results of C_1 and C_3 is in an acceptable range.

Capacitance C_2 inside the NC solid is evaluated by using a mutual capacitance between two Si NCs in 7-nm diameter. Mutual capacitance between two spheres in a radius r can be expressed as,

$$C = 4\pi\epsilon r \sinh\beta \sum_{n=1}^{\infty} \frac{1}{\sinh 2n\beta}, \tag{4}$$

where β is defined to be acosh($d'/2r$), and d' is a distance between the center of each sphere (Figure S3(b)).[37,39,40] Combined capacitance inside the solid is 4.0 nF (the detailed calculation is shown in the supplementary material).[38] This value is smaller than the experimental C_2, but still within an acceptable range by considering the crudeness of the model.

We also show that the impedance plot is not dependent on a DC bias voltage and 405-nm light irradiation in Figs. S4(a) and S4(b).[38] All of the fitted parameters and evaluated time constant ($\tau_i = R_i C_i$) are nearly constant in Figs. S4(c)–S4(e). The time constant in the NC solid (τ_2) is around

TABLE I. Equivalent circuit parameters of an Al/Si-NC solid/ITO layered structure in Fig. 6(a).

Interface of ITO/Si-NC solid (J_1)		A Si-NC solid (J_2)		Interface of Si-NC solid/Al (J_3)	
R_1	C_1	R_2	C_2	R_3	C_3
141 kΩ	54.6 nF	101 MΩ	13.4 nF	890 kΩ	79.8 nF

3 s, which clearly corresponds to the decay constant of the photocurrent in Fig. 3(a). These results imply that most of V_{DC} are applied to a Si-NC solid due to its high resistivity, which dominates the carrier transport. As shown above, the equivalent circuit obtained by impedance spectroscopy easily provides us the similar information about a NC solid in DC transport analysis.

IV. CONCLUSIONS

In conclusion, we analyze the electrical properties of NC solids by using both an energy band diagram and an equivalent circuit. DC transport of a NC solid indicates that charge carriers are tunneling through tunneling barriers in the solid. Photocurrent generation is enhanced by applying a higher electric field because of the Fowler-Nordheim tunneling process. Conductive AFM images of a NC solid show that a current through the solid is strongly dependent on the thickness, which also indicates the tunneling transport. Impedance spectroscopy reveals the equivalent circuit of NC solids between ITO and Al. It is a three series of parallel resistor-capacitors corresponding to ITO/NC, NC/NC, and NC/Al. The obtained circuit parameters are explained by a simple structural model. As a result, impedance spectroscopy can be a useful technique to analyze semiconductor NC solids as well as usual DC transport. The combined analysis of the energy band diagram and the equivalent circuit will be indispensable to obtain information necessary to implement NC solids into actual electronic devices.

ACKNOWLEDGMENTS

The authors thank Dr. K. Imakita for discussion regarding the results. This work was partly supported by KAKENHI (26886008 and 16H03828), 2014 JSPS Bilateral Joint Research Projects (Japan-Czech Republic), Visegrad Group (V4)-Japan Joint Research Project on Advanced Materials "NaMSeN". Measurements on a conductive AFM and a stylus profiler were supported by "Nanotechnology Platform Project (Nanotechnology Open Facilities in Osaka University)" of Ministry of Education, Culture, Sports, Science, and Technology, Japan [No. S-15-OS-0033].

[1] A. Zabet-Khosousi and A.-A. Dhirani, Chem. Rev. **108**, 4072 (2008).
[2] D. V. Talapin, MRS Bull. **37**, 63 (2012).
[3] S. Kano, T. Tada, and Y. Majima, Chem. Soc. Rev. **44**, 970 (2015).
[4] C. R. Kagan and C. B. Murray, Nat. Nanotechnol. **10**, 1013 (2015).
[5] P. Guyot-Sionnest, J. Phys. Chem. Lett. **3**, 1169 (2012).
[6] N. Rastgar and D. Rowe, J. Phys. Chem. C **117**, 4211 (2013).
[7] R. N. Pereira, S. Niesar, W. B. You, A. F. Da Cunha, N. Erhard, A. R. Stegner, H. Wiggers, M. G. Willinger, M. Stutzmann, and M. S. Brandt, J. Phys. Chem. C **115**, 20120 (2011).
[8] M. A. Rafiq, Y. Tsuchiya, H. Mizuta, S. Oda, S. Uno, Z. A. K. Durrani, and W. I. Milne, J. Appl. Phys. **100**, 014303 (2006).
[9] T. Chen, K. V. Reich, N. J. Kramer, H. Fu, U. R. Kortshagen, and B. I. Shklovskii, Nat. Mater. **15**, 299 (2016).
[10] T. Burr, a. Seraphin, E. Werwa, and K. Kolenbrander, Phys. Rev. B **56**, 4818 (1997).
[11] T. Chen, B. Skinner, W. Xie, B. I. Shklovskii, and U. R. Kortshagen, J. Phys. Chem. C **118**, 19580 (2014).
[12] K. Mohanta, S. K. Majee, S. K. Batabyal, and A. J. Pal, J. Phys. Chem. B **110**, 18231 (2006).
[13] J. Huh, J. Na, J. S. Ha, S. Kim, and G. T. Kim, ACS Appl. Mater. Interfaces **3**, 3097 (2011).
[14] K. Slowinski and M. Majda, J. Electroanal. Chem. **491**, 139 (2000).
[15] C. S. S. Sangeeth, A. Wan, and C. a Nijhuis, J. Am. Chem. Soc. **136**, 11134 (2014).
[16] M. Sugiyama, M. Hayashi, C. Yamazaki, N. B. Hamidon, Y. Hirose, and M. Itagaki, Thin Solid Films **535**, 287 (2013).
[17] A. K. Rath, T. Lasanta, M. Bernechea, S. L. Diedenhofen, and G. Konstantatos, Appl. Phys. Lett. **104**, 063504 (2014).
[18] D. P. Puzzo, E. J. Henderson, M. G. Helander, Z. Wang, G. A. Ozin, and Z. Lu, Nano Lett. **11**, 1585 (2011).
[19] J. Liu, C. Fan, X. Chen, G. Jiao, C. Hu, and Y. Qian, Mater. Sci. Semicond. Process. **20**, 12 (2014).
[20] I.-H. Chu, M. Radulaski, N. Vukmirovic, H.-P. Cheng, and L.-W. Wang, J. Phys. Chem. C **115**, 21409 (2011).
[21] R. Gresback, N. J. Kramer, Y. Ding, T. Chen, U. R. Kortshagen, and T. Nozaki, ACS Nano **8**, 5650 (2014).
[22] T. Lin, X. Liu, B. Zhou, Z. Zhan, A. N. Cartwright, and M. T. Swihart, Adv. Funct. Mater. **24**, 6016 (2014).
[23] H. Sugimoto, M. Fujii, K. Imakita, S. Hayashi, and K. Akamatsu, J. Phys. Chem. C **116**, 17969 (2012).
[24] H. Sugimoto, M. Fujii, K. Imakita, S. Hayashi, and K. Akamatsu, J. Phys. Chem. C **117**, 11850 (2013).
[25] H. Sugimoto, M. Fujii, K. Imakita, S. Hayashi, and K. Akamatsu, J. Phys. Chem. C **117**, 6807 (2013).
[26] M. Fujii, H. Sugimoto, M. Hasegawa, and K. Imakita, J. Appl. Phys. **115**, 084301 (2014).
[27] K. Furuta, M. Fujii, H. Sugimoto, and K. Imakita, J. Phys. Chem. Lett. **6**, 2761 (2015).
[28] Y. Hori, S. Kano, H. Sugimoto, K. Imakita, and M. Fujii, Nano Lett. **16**, 2615 (2016).
[29] M. Sasaki, S. Kano, H. Sugimoto, K. Imakita, and M. Fujii, J. Phys. Chem. C **120**, 195 (2016).
[30] D. Nečas and P. Klapetek, Open Phys. **10**, 181 (2012).
[31] J. G. Simmons, J. Appl. Phys. **34**, 2581 (1963).
[32] M. Lenzlinger and E. Snow, J. Appl. Phys. **40**, 278 (1969).
[33] E. Z. Luo, J. B. Xu, W. Wu, I. H. Wilson, B. Zhao, and X. Yan, Appl. Phys. A **66**, S1171 (1998).
[34] S. Banerjee, M. A. Salem, and S. Oda, Appl. Phys. Lett. **83**, 3788 (2003).
[35] J. Y. Son and Y.-H. Shin, Appl. Phys. Lett. **92**, 222106 (2008).
[36] A. Singh and A. Chandra, Sci. Rep. **5**, 15551 (2015).
[37] W. R. Smythe, *Static and Dynamic Electricity* (McGraw-Hill, 1950).
[38] See supplementary material at http://dx.doi.org/10.1063/1.4953216 for additional information.
[39] J. Lekner, J. Appl. Phys. **111**, 076102 (2012).
[40] S. Kano, K. Maeda, D. Tanaka, M. Sakamoto, T. Teranishi, and Y. Majima, J. Appl. Phys. **118**, 134304 (2015).